According to (13), if power $|A|^2$ enters port 1, then power $A^2|S_{31}|^2$ will come out port 3, and if power A^2 is put in port 2, power $|A|^2|S_{22}|^2=|A|^2|S_{31}|^2$ will be reflected. This is precisely the result sought.

A special case of this result, obtained by Aitken and McLean [8], states that, if the junction is symmetric, the power reflected at port 1 and the power out port 3 will be equal. This follows since, if the junction is symmetric, $S_{11}=S_{22}$ and $|A|^2|S_{31}|^2=|A|^2|S_{11}|^2$.

The fact that the derivation of (13) did not require symmetry makes the result particularly useful to the experimentalist since he will, in general, be dealing with junctions that are not truly symmetric.

Acknowledgment

The author wishes to acknowledge the assistance of W. Passaro and D. Landry in the development of these devices and Dr. G. Burdick, who contributed greatly in providing the theoretical background and guidance throughout the program.

References

[1] Milano, U., J. H. Saunders, and L. Davis, Jr., A Y-junction strip-line circulator, *IRE Trans. on Microwave Theory and Techniques*, vol MTT-8, May 1960, pp 346–350.
[2] Clark, J., Perturbation techniques for miniaturized coaxial Y-junction circulators, *J. Appl. Phys.*, suppl. to vol 32, Mar 1961, p 323s–324s.
[3] Clark, J., and J. Brown, Miniaturized, temperature stable coaxial Y-junction circulators, *IRE Trans. on Microwave Theory and Techniques*, vol MTT-9, May 1961, pp 267–269.
[4] Auld, B. A., The synthesis of symmetrical waveguide circulators, *IRE Trans. on Microwave Theory and Techniques*, vol MTT-7, Apr 1959, pp 238–246.
[5] Bosma, H., On the principle of stripline circulation, *Proc. IEE (London)*, vol 109, pt B, suppl. no 21, Jan 1963, p 137–146.
[6] ——, On stripline Y-circulation at UHF, *IEEE Trans. on Microwave Theory and Techniques*, vol MTT-12, Jan 1964, pp 61–72.
[7] Humphreys, B. L., and J. B. Davies, The synthesis of N-port circulators, *IRE Trans. on Microwave Theory and Techniques*, vol MTT-10, Nov 1962, pp 551–554.
[8] Aitken, F. M., and R. McLean, Some properties of the waveguide Y-circulator, *Proc. IEE (London)*, Feb 1963, pp 256–260.
[9] Montgomery, C., R. H. Dicke, and E. M. Purcell, *Principles of Microwave Circuits*. New York: McGraw-Hill, 1948, ch 12.

Generalized Plots of Mode Patterns in a Cylindrical Dielectric Waveguide Applied to Retinal Cones

G. BIERNSON, SENIOR MEMBER, IEEE, AND D. J. KINSLEY

Abstract—**Generalized curves are presented which describe the characteristics of the 12 lowest cutoff-frequency modes of an electromagnetic wave propagating down an infinite lossless dielectric rod, surrounded by an infinite lossless medium of lower dielectric constant. These curves were developed by a computer study particularly to analyze the optical mode patterns generated within the photosensitive portions of the cones of the retina. However, they should also be particularly useful in the study of fiber optics and dielectric microwave antennas.**

I. Introduction

A DIELECTRIC rod surrounded by a medium of lower dielectric constant acts as a waveguide. However, the characteristics of the modes propagated in such a waveguide are more complex than in the more familiar metallic waveguide case because 1) part of the energy propagates outside the dielectric rod, and 2) the spatial distribution of the energy in a mode varies with wavelength. In a metallic waveguide, all the energy is contained within the waveguide, and the shape of a mode is the same over the frequency range at which it can exist.

Stratton [1] has shown that the characteristics of the modes can be obtained by solving a complicated transcendental equation containing Bessel and Hankel functions. Snitzer [2] has discussed the nature of the modes which arise from solutions of this equation. This paper presents the results of a digital computer solution of this equation, which has provided a series of generalized curves describing the characteristics of the 12 modes having the lowest cutoff frequencies. This approach can be extended to include other modes. The spatial distribution of energy in a given mode is characterized by a Bessel function of a particular order. For each mode, the Bessel-function argument at the boundary of the rod (designated u) is plotted vs. a nondimensional fre-

Manuscript received August 3, 1964; revised February 1, 1965. The work reported herein was sponsored under contract AF-33(657)-11717 with the Aerospace Medical Research Laboratories, Air Force Systems Command, U. S. Air Force.

The authors are with the Applied Research Lab., Sylvania Electronic Systems, a Div. of Sylvania Electric Products Inc., Waltham, Mass.

quency v for selected values of relative dielectric constant δ. From these curves, the Bessel-function argument at the boundary of the rod can be found at any frequency, and this specifies the actual energy distribution in the rod.

The analysis of the cylindrical dielectric waveguide appears to have a practical application in the study of the mechanism of color vision in the human eye. The photosensitive portions of the visual receptors of the retina are cylindrical structures having radii roughly equal to a wavelength of light. With such small radii, these cylindrical structures should be considered to be dielectric waveguides, since light can propagate down them in only a few modes. Enoch [3], [4] has observed, from light emanating from the tips of the receptors, waveguide mode patterns corresponding to the 12 modes having the lowest cutoff frequencies.

There is good reason to believe that these waveguide effects in the photosensitive portions of the cones may produce spectral discrimination in color vision [5]. The purpose of this study of waveguide modes has been to explore this possibility by determining the energy distributions across the receptor produced by particular waveguide modes, as a function of wavelength.

II. General Results

We are considering the case of an infinite lossless dielectric rod, which we will call the core, surrounded by an infinite dielectric medium of lower dielectric constant, which we will call the cladding. Our problem is to determine the characteristics of modes that are capable of propagating in this structure.

Appendix A presents a derivation of equations describing the characteristics of the modes. These were evaluated by a digital computer program (which is discussed in Appendix B) to produce generalized curves for the 12 modes with the lowest cutoff frequencies. To help orient the reader, this section presents a simple set of curves which provide approximate values for the characteristics of the modes. Section III presents a complete set of curves for precise calculation.

Within the core, the electric and magnetic field vectors for a mode are represented by Bessel-function expressions. We will describe the characteristics of a mode by specifying the parameter u, defined as the argument of the Bessel function at the boundary between the core and cladding (i.e., at the circumference of the dielectric rod). For the case of a small difference in dielectric constant between core and cladding, each mode can be approximately described by a single curve relating the parameter u to a nondimensional frequency v. The nondimensional frequency v is proportional to the actual frequency ν of the electromagnetic wave and is defined as

$$v = (2\pi a/c)\sqrt{\epsilon_1' - \epsilon_2'} \quad \nu = 2\pi\sqrt{\epsilon_1' - \epsilon_2'}\,(a/\lambda) \quad (1)$$

where

ν = optical frequency in c/s,
λ = wavelength,
a = radius of core,
n_1 = index of refraction of core,
n_2 = index of refraction of cladding,
$\epsilon_1' = n_1^2$ = dielectric constant of core,
$\epsilon_2' = n_2^2$ = dielectric constant of cladding,
c = speed of light.

Figure 1 gives the approximate plots of u, the Bessel-function argument at the boundary, vs. the nondimensional frequency v for the 12 modes with the lowest cutoff frequencies. These curves hold approximately for the case of a small difference in dielectric constant between core and cladding. As is shown, a number of modes have the same approximate plot of u vs. v for this case. These modes also have approximately the same energy distribution plots for this case, although the E-field and H-field plots are different.

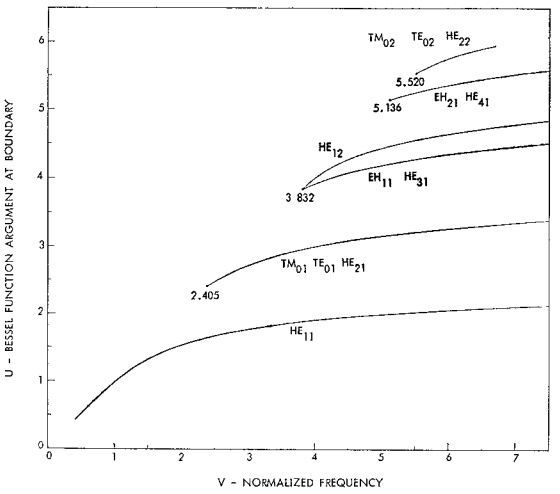

Fig. 1. Plots for $\delta = 0$ of Bessel-function argument u at boundary vs. nondimensional frequency v for the various modes.

To obtain a precise value for u, we can describe each mode by a family of curves, each one corresponding to a particular ratio of dielectric constant of the core to dielectric constant of the cladding. It is convenient to express this ratio in terms of the parameter δ, defined as

$$\delta = (\epsilon_1' - \epsilon_2')/\epsilon_1' = (n_1^2 - n_2^2)/n_1^2. \quad (2)$$

Section III gives for each of the 12 modes a family of curves of u vs. v for values of δ from 0 to 0.5.

The approximate curves of u vs. v in Fig. 1 represent the limiting case where δ approaches zero, which we express simply as $\delta = 0$. Although the $\delta = 0$ case is unrealistic, the curves of u vs. v which result for small but realistic values of δ are not much different from the curve for $\delta = 0$, which is also shown in Section III.

For a particular mode, the electric E-field and magnetic H-field components along the direction of propagation (called the z direction) are proportional to

$$E_z = J_n(ur/a) \cos n\theta \exp\{i[h'(z/a) - \omega t]\} \quad (3)$$

$$H_z = \alpha J_n(ur/a) \sin n\theta \exp\{i[h'(z/a) - \omega t]\} \quad (4)$$

where

n = integer from 0 to ∞ representing order of mode
J_n = Bessel function of nth order
r = radial distance from axis of core
z = distance measured along axis of core
θ = angle measured about axis of core
$\omega = 2\pi\nu$ = angular frequency of optical wave
α = a constant
h' = normalized propagation constant.

The constant h' is equal to

$$h' = \sqrt{(1/\delta)v^2 - u^2}. \quad (5)$$

For each value of u, the transcendental equation that characterizes the modes has two infinite sets of solutions, which define two sets of modes. For $n \geq 0$, the two sets of modes are labeled HE_{nm} and EH_{nm}, where the subscript m takes on integer values from one to infinity. Snitzer [2] gives a detailed discussion of the basis for this nomenclature. For $n = 0$, the two sets of modes are labeled TE_{nm} and TM_{nm} or specifically TE_{0m} and TM_{0m}.

The TE_{0m} and TM_{0m} modes are called transverse electric and transverse magnetic modes, respectively, because the electric E field for a TE_{0m} mode is completely transverse (there is *no* E-field component in the direction of propagation), and the magnetic H field for a TM_{0m} mode is completely transverse. The EH_{nm} and HE_{nm} are called hybrid modes because they have both E and H fields along the direction of propagation.

As was shown in (3) and (4) the subscript n is an integer (from zero to infinity) that establishes the order of the Bessel function describing the E_z- or H_z-field components. For each value of n there are two infinite sets of modes, labeled TE_{0m} and TM_{0m} for $n = 0$, or HE_{nm} and EH_{nm} for $n \geq 1$. The parameter m varies from one to infinity and designates the sequence of a particular mode in either of these infinite sets. To solve for the parameters of the modes, an oscillatory Bessel-function expression is approximately equated to a monotonically decaying Hankel function expression. A separate solution occurs at every cycle of the Bessel function (except possibly the first cycle), and the parameter m describes which of these solutions is being considered.

The higher the values of n and m, the higher is the cutoff frequency for the mode. In those situations where the mode concept is useful, there are usually only a few modes that are above cutoff in the frequency range of interest.

The power being propagated along the waveguide is characterized by the power density along the z direction, denoted S_z. If the value of δ is small, as in the case of retinal receptors, the power density S_z for an individual mode is not a function of z or θ, but varies only with the radial distance r. Within the core the energy density is proportional to

$$S_z \propto [J_{n\pm1}(ur/a)]^2 \qquad \text{for } r \leq a \quad (6)$$

where the plus sign holds for EH modes, the minus sign for HE modes. For the TE and TM modes, either sign can be used, because for $n = 0$ the expressions for both signs are equal.

In the cladding, the field is characterized by Hankel functions. The power density propagating in the Z direction is proportional to

$$S_z \propto [K_{n\pm1}(wr/a)]^2 \qquad \text{for } r \geq a \quad (7)$$

where the parameter w is defined as

$$w = \sqrt{v^2 - u^2}. \quad (8)$$

Again, in (7) the plus sign holds for the EH modes, the minus sign for the HE modes, and either sign may be used for the TE and TM modes. The function K_p represents the pth-order modified Hankel function. This function is positive for positive argument and decays monotonically to zero with increasing positive argument. For small values of δ there is no discontinuity of power density S_z across the boundary between core and cladding.

Figure 2 gives normalized plots of $J_p^2(x)$, for $p = 0$, 1, 2, 3. By (6), these can be used to form plots of power density S_z as functions of radial distance for the various modes by noting that the value $x = u$ corresponds to the boundary between core and cladding. The modes corresponding to the particular values of p are indicated.

It is often convenient to consider the power falling within an annular ring of constant width, which is proportional to (rS_z). For this purpose, Fig. 3 gives normalized plots of $xJ_p^2(x)$ for $p = 0$, 1, 2, 3, which can be used to obtain plots of power density within an annular ring.

When more than one mode is present, interference between the modes can occur, and the power density S_z can vary with θ and z as well as with r. Nevertheless, if we consider the total power propagating through an annular ring, averaged over the axial distance z, the interference effects between modes would cancel out, and the plots of Fig. 3 would still apply to individual modes in this average sense.

III. Detailed Plots

For the 12 modes being considered, Figs. 4 to 13 give plots of the Bessel-function argument u at the boundary between core and cladding vs. the nondimensional fre-

quency v, for values of δ equal to 0, 0.1, 0.2, 0.3, 0.4, and 0.5. The TE_{01} and TE_{02} modes are not a function of δ, and so the plots of u vs. v for these modes are the same as the plots for the TM_{01} and TM_{02} modes at $\delta = 0$.

If the dielectric constant of the core and cladding and the radius of the core are known, one can find the value for δ and the value for v for a given optical frequency. Applying these values to Figs. 4 to 13 gives the values of u for the various modes. These values of u can then be applied to the corresponding energy distribution plots for those modes given in Figs. 2 and 3 to form plots of power density and power within an annular ring as functions of radius. The value for u represents the value of x in Figs. 2 and 3 corresponding to the boundary between core and cladding. By stretching the horizontal scales of Figs. 2 and 3 so that the values $x = u$ coincide for all the modes, plots of the power distributions are formed.

At the cutoff frequency, all the energy propagates within the cladding outside the core. As the frequency increases, a larger and larger fraction of the energy propagates within the core. It is convenient to define a waveguide efficiency η as the relative power propagating with the core. The efficiency η is defined as

$$\eta = \frac{\text{power propagating within core}}{\text{total propagating power}}. \tag{9}$$

Figures 14 and 15 give plots of η for the various modes as functions of normalized frequency v for the conditions $\delta = 0$ and $\delta = 0.4$. For the TE_{01} and TE_{02} modes, use the curves for TM_{01} and TM_{02} at $\delta = 0$.

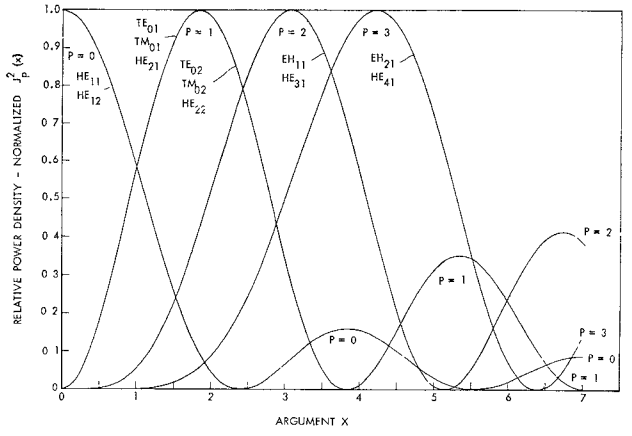

Fig. 2. Curves for forming plots of relative power density vs. radius for the various modes.

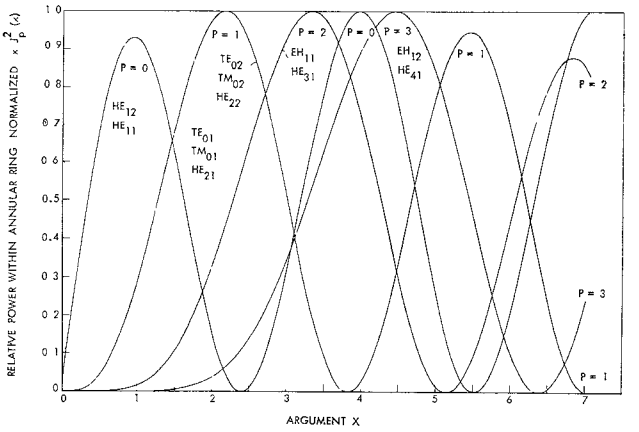

Fig. 3. Curves for forming plots of power within an annular ring vs. radius for the various modes.

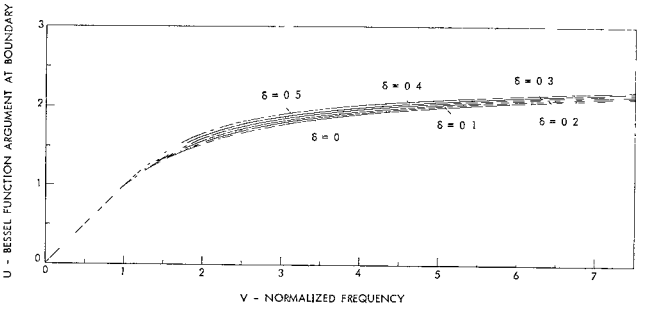

Fig. 4. Plots of Bessel-function argument u at boundary vs. nondimensional frequency V for HE_{11} mode.

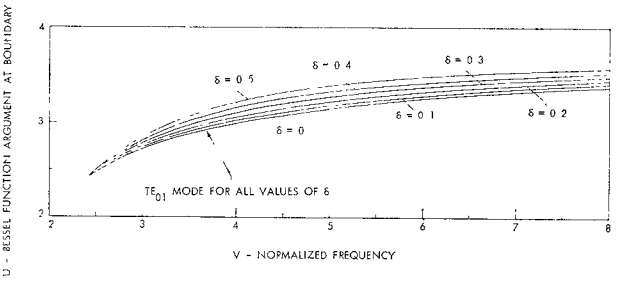

Fig. 5. Plots of Bessel-function argument u at boundary vs. nondimensional frequency V for TM_{01} and TE_{01} modes.

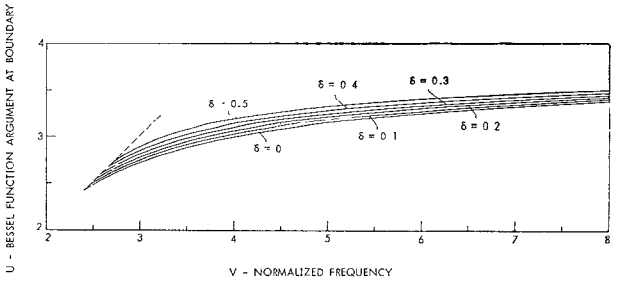

Fig. 6. Plots of Bessel-function argument u at boundary vs. nondimensional frequency V for HE_{21} mode.

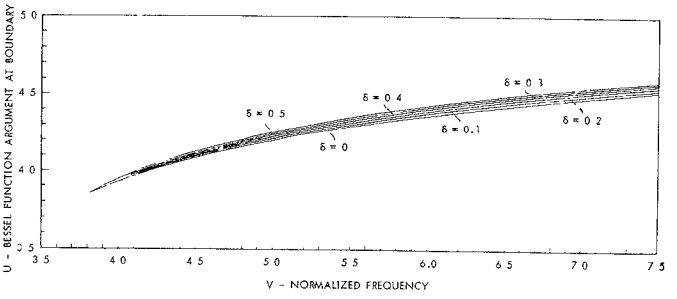

Fig. 7. Plots of Bessel-function argument u at boundary vs. nondimensional frequency V for EH_{11} mode.

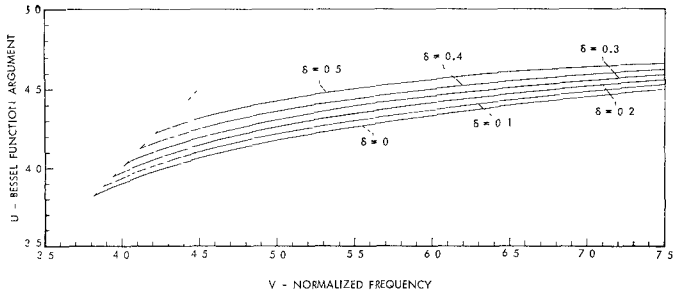

Fig. 8. Plots of Bessel-function argument u at boundary vs. nondimensional frequency V for HE_{31} mode.

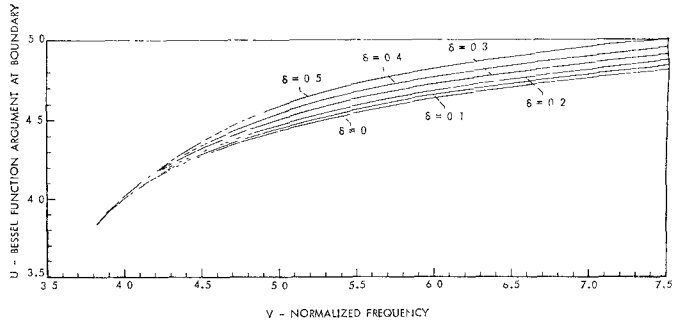

Fig. 9. Plots of Bessel-function argument u at boundary vs. nondimensional frequency V for HE_{12} mode.

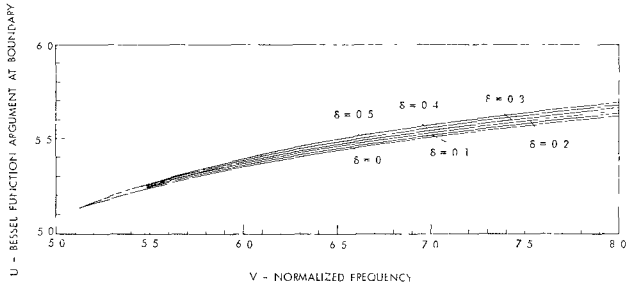

Fig. 10. Plots of Bessel-function argument u at boundary vs. nondimensional frequency V for EH_{21} mode.

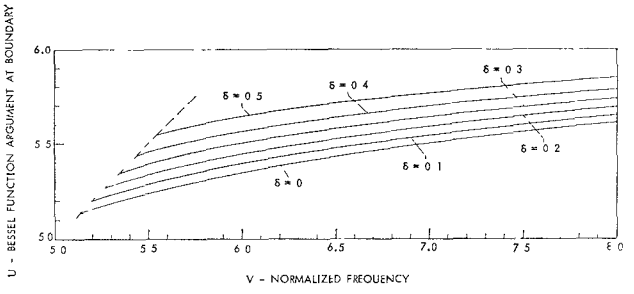

Fig. 11. Plots of Bessel-function argument u at boundary vs. nondimensional frequency V for HE_{41} mode.

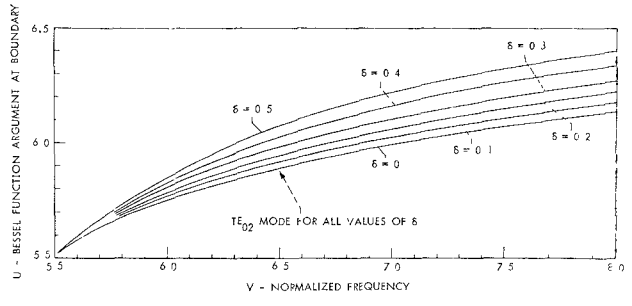

Fig. 12. Plots of Bessel-function argument u at boundary vs. nondimensional frequency V for TM_{02} and TE_{02} modes.

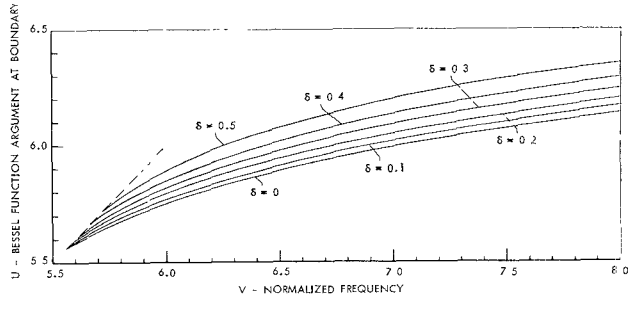

Fig. 13. Plots of Bessel-function argument u at boundary vs. nondimensional frequency V for HE_{22} mode.

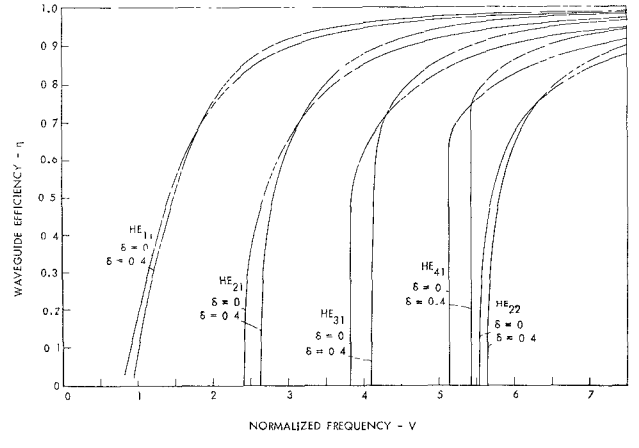

Fig. 14. Plots for $\delta=0$ and $\delta=0.4$ of waveguide efficiency η vs. normalized frequency V for HE_{11}, HE_{21}, H_{31}, HE_{41}, and HE_{22} modes.

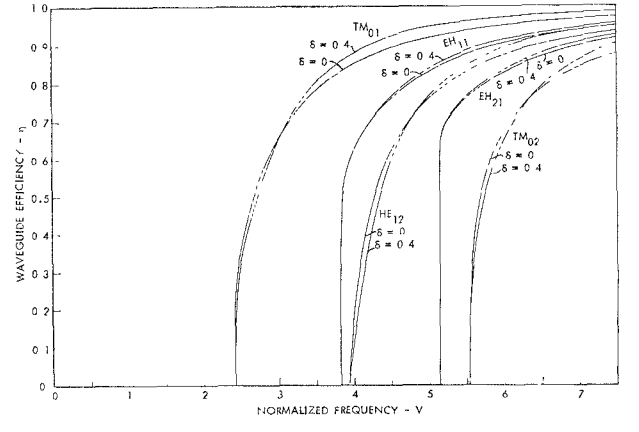

Fig. 15. Plots for $\delta=0$ and $\delta=0.4$ of waveguide efficiency η vs. normalized frequency V for TM_{01}, EH_{11}, HE_{12}, EH_{21}, and TM_{02} modes.

IV. Field Vectors

If the value of u is known for a given mode at a given frequency, the field-vector plots can be obtained from the following equations. Let us define parameters

$$w = \sqrt{v^2 - u^2} \tag{10}$$

$$h' = \sqrt{(1/\delta)v^2 - u^2} \tag{11}$$

$$F = \exp\{i[h'(z/a) - \omega t]\} \tag{12}$$

$$p = \frac{n(1/u^2 + 1/w^2)}{[J_n'(u)/uJ_n(u)] + [K_n'(w)/wK_n(w)]} \tag{13}$$

$$P_2 = \frac{n(1/u^2 + 1/w^2)}{[J_n'(u)/uJ_n(u)] + (1-\delta)[K_n'(w)/wK_n(w)]} \tag{14}$$

$$P_3 = (1-\delta)P_2 \tag{15}$$

$$\alpha = h'P_1/\mu_0\omega a \tag{16}$$

$$\beta = J_n(u)/K_n(w) \tag{17}$$

where $J_n'(u)$ and $K_n'(w)$ are the derivatives of $J_n(u)$ and $K_n(w)$. An alternate expression for α is

$$\alpha = \epsilon_0 c n_1 \sqrt{1 - \delta(u/v)^2}\, P_1 \tag{18}$$

where n_1 is the index of refraction of the core. The E and H fields for a particular mode can be shown to be as follows inside the core

$$E_z = J_n F \cos n\theta \tag{19a}$$

$$E_r = i(h'/2u)[(1-P_1)J_{n-1} + (1+P_1)J_{n+1}]F \sin n\theta \tag{19b}$$

$$E_\theta = -i(h'/2u)[(1-P_1)J_{n-1} + (1+P_1)J_{n+1}]F \sin n\theta \tag{19c}$$

$$H_z = -\alpha J_n R \sin n\theta \tag{20a}$$

$$H_r = -i\alpha(h'/2u)[(1-P_2)J_{n-1} - (1+P_2)J_{n+1}]F \sin n\theta \tag{20b}$$

$$H_\theta = -i\alpha(h'/2u)[(1-P_2)J_{n-1} + (1+P_2)J_{n+1}]F \cos n\theta \tag{20c}$$

where the argument of J is (ur/a). Outside the core the fields are

$$E_z = \beta K_n F \cos n\theta \tag{21a}$$

$$E_r = i\beta(h'/2w)[(1-P_1)K_{n-1} + (1+P_1)K_{n+1}]F \cos n\theta \tag{21b}$$

$$E_\theta = -i\beta(h'/2w)[(1-P_1)K_{n-1} - (1+P_1)K_{n+1}]F \sin n\theta \tag{21c}$$

$$H_z = -\alpha\beta K_n F \sin n\theta \tag{22a}$$

$$H_r = -i\alpha\beta(h'/2w)[(1-P_3)K_{n-1} + (1+P_3)K_{n+1}]F \sin n\theta \tag{22b}$$

$$H_\theta = -i\alpha\beta(h'/2w)[(1-P_3)K_{n-1} - (1+P_3)K_{n+1}]F \cos n\theta \tag{22c}$$

where the argument of K is (wr/a).

The quantity ϵ_0 is the permittivity of free space, and the coordinates are:

1) r = radial distance from axis of rod
2) z = distance measured along axis of rod
3) θ = angle measured around axis of rod.

These equations hold for one particular power level in the mode. The angle θ and the distance z are measured relative to angular and linear references that are established by the particular characteristics of the mode, which depend on the way the dielectric rod is excited.

The equation for power propagating in the z direction per unit area is

$$S_z = 1/2(E_r H_\theta - E_\theta H_r). \tag{23}$$

Since we are interested only in waves propagating along the core, this is the power density of interest. For small values of δ, the power density S_z varies only with radius and is approximately continuous across the boundary between the core and cladding. If the power of each mode is normalized such that the power density at the boundary is unity, the expression for power density for small δ then becomes

$$S_z = [J_{n\pm1}(ur/a)/J_{n\pm1}(u)]^2 \qquad r < a \tag{24}$$

$$S_z = [K_{n\pm1}(wr/a)/K_{n\pm1}(w)]^2 \qquad r > a \tag{25}$$

where the plus sign holds for EH modes and the minus sign for HE modes, and either sign can be used for the TE and TM modes.

V. Application of Curves to Retinal Cones

The outer segments of the retinal cones, which presumably perform the photo-detection process, are long cylinders about one micron in diameter. Enoch [3], [4] has observed mode patterns by examining the light emanating from the ends of the outer segments of the cones when the retina is illuminated. From these observations, he was able to determine the presence of at least one mode in each of the following six sets of modes combined within parentheses: (HE_{11}), (TM_{01}, TE_{01}, HE_{21}), (EH_{11}, HE_{31}), (HE_{12}), (EH_{21}, HE_{41}), (TM_{02}, TE_{02}, HE_{22}). As shown previously, the modes in a given set have approximately the same plots of power density vs. radius.

From Enoch's observations we can estimate the dielectric characteristics of the cones by assuming that 1) the cutoff frequencies of all the modes he observes lie within or below the visual frequency range, and 2) modes he does not observe have cutoff frequencies above the visual frequency range. For these assumptions, reasonable estimates of the indexes of refraction of the outer segment of the cone and surrounding medium are $n_1 = 1.5$ and $n_2 = 1.3$. The value for δ would then be 0.25. For a radius of $a = 0.5$ micron, the cutoff wavelengths for the modes observed by Enoch would be approximately as follows: HE_{11} mode, infinity; (TM_{01}, TE_{01}, HE_{21}) modes, 980 mμ; (EH_{11}, HE_{31}) modes, 610 mμ; HE_{12} mode, 610 mμ; (EH_{21}, HE_{41}) modes, 450 mμ; (TM_{02}, TE_{03}, HE_{22}) modes, 420 mμ. The next higher set of modes is (EH_{31}, HE_{51}), which has a normalized cutoff frequency for $\delta = 0$ of 5.52. The cutoff wavelength would be 370 mμ, which lies below the visible wavelength range.

Figures 16 to 21 gives normalized plots of power density vs. radius for the HE_{11}, TM_{01}, EH_{11}, HE_{12}, EH_{21}, and TM_{02} modes at specific wavelengths for the assumed dielectric parameters of the retinal cones ($a = 0.5$ micron, $n = 1.5$, $n_2 = 1.3$, $\delta = 0.25$). The power density plots for

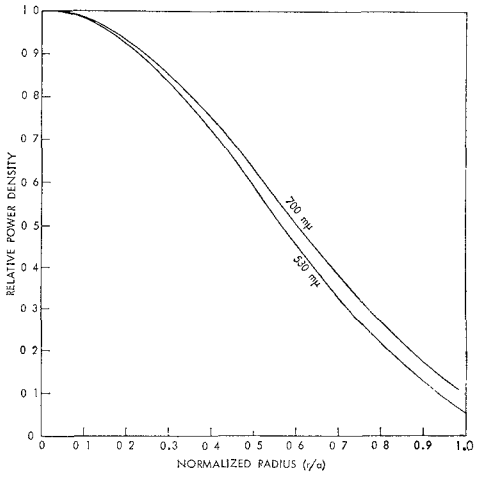

Fig. 16. Plots of power density vs. radius in the retinal cones for HE_{11} mode, based on assumed dielectric characteristics.

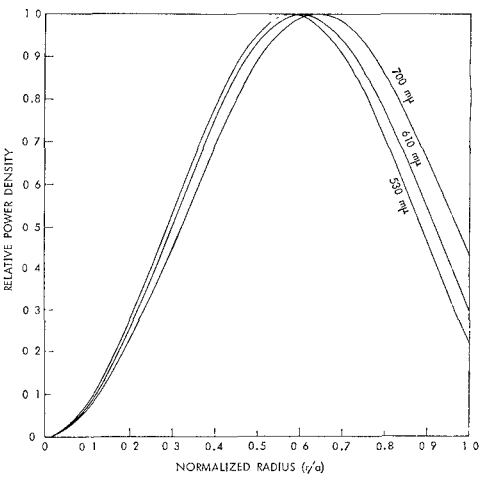

Fig. 17. Plots of power density vs. radius in the retinal cones for TM_{01} mode, based on assumed dielectric characteristics.

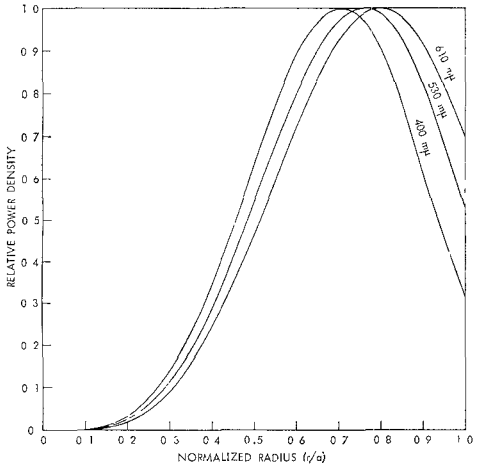

Fig. 18. Plots of power density vs. radius in the retinal cones for EH_{11} mode, based on assumed dielectric characteristics.

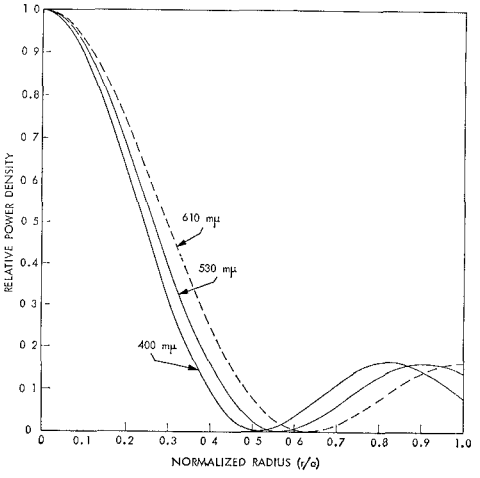

Fig. 19. Plots of power density vs. radius in the retinal cones for HE_{12} mode, based on assumed dielectric characteristics.

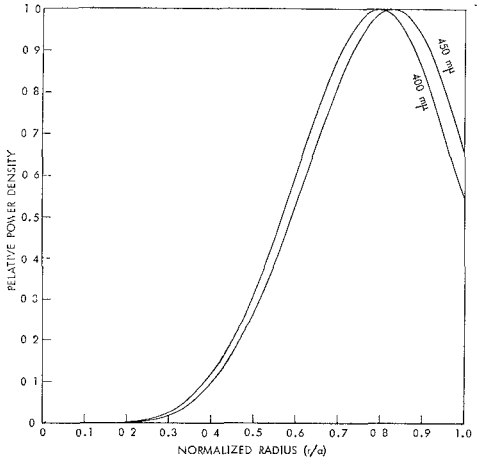

Fig. 20. Plots of power density vs. radius in the retinal cones for EH_{21} mode, based on assumed dielectric characteristics.

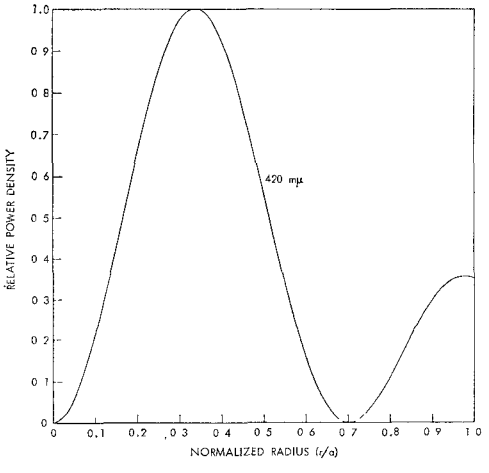

Fig. 21. Plots of power density vs. radius in the retinal cone for TM_{02} mode, based on assumed dielectric characteristics.

the TE_{01} and HE_{21} modes are approximately the same as those for the TM_{01} mode; the plots for the HE_{31} mode are approximately the same as those for EH_{11} mode, etc.

If we examine the plots of mode efficiency in Figs. 14 and 15, we find that they are zero at cutoff and for most modes rise rapidly as frequency is increased above cutoff. However, for the HE_{11} and HE_{12} modes, the mode efficiency stays practically zero until a significantly higher frequency. Thus we should consider the HE_{11} and HE_{12} modes as having effective cutoff frequencies that are higher than the theoretical values are consequently the plot in Fig. 19 for HE_{21} mode at its theoretical cutoff frequency 610 mμ is indicated by a dashed curve, since this curve does not have much physical meaning.

Appendix A

Equations for Waveguide Modes in a Dielectric Rod

Let us consider a dielectric waveguide consisting of an infinite cylindrical core of radius a and dielectric constant ϵ_1' surrounded by cladding of lower dielectric constant ϵ_2' where both regions are perfect insulators with a free-space magnetic permeability μ_0. Choose a cylindrical coordinate system r, θ, z, with the z axis lying along the axis of the cylinder. Waves that propagate down such a structure can be expressed as a sum of a finite number of waveguide modes. Snitzer [2] shows that, for a single mode, the z components of the field within the core can be expressed as

$$E_z = A_n J_n(ur/a) \cos(n\theta + \phi_n) \exp\{i(hz - \omega t)\} \quad (26)$$

$$H_z = B_n J_n(ur/a) \cos(n\theta + \psi_n) \exp\{i(hz - \omega t)\}. \quad (27)$$

The z components of the field within the cladding are

$$E_z = C_n K_n(wr/a) \cos(n\theta + \phi_n) \exp\{i(hz - \omega t)\} \quad (28)$$

$$H_z = D_n K_n(wr/a) \cos(n\theta + \psi_n) \exp\{i(hz - \omega t)\}. \quad (29)$$

The function J_n is the Bessel function of the first kind, and K_n is the modified Hankel function of the first kind which is related to the Hankel function of the first kind $H_n^{(1)}$ by

$$K_n(w) = (\pi/2) i^{n+1} H_n^{(1)}(iw). \quad (30)$$

The Bessel and Hankel functions are commonly tabulated [6] only for n equal to 0 and 1. The values for other orders of n can be found from the relations

$$J_{n+1}(u) + J_{n-1}(u) = 2(n/u) J_n(u) \quad (31)$$

$$K_{n+1}(w) - K_{n-1}(w) = 2(n/w) K_n(w) \quad (32)$$

$$J_{-n} = (-1)^n J_n \quad (33)$$

$$K_{-n} = K_n. \quad (34)$$

All the modified Hankel functions are positive and decay monotonically to zero as the argument increases. The Bessel functions have the form of damped oscillations. The derivatives of the Bessel and Hankel functions are given by

$$2J_n' = J_{n-1} - J_{n+1} \quad (35)$$

$$-2K_n' = K_{n-1} + K_{n+1}. \quad (36)$$

For small values of w the modified Hankel function can be approximated by

$$K_0(w) \cong \mathrm{Ln}\,(2/\gamma w), \quad \text{where } \gamma = 1.781 \text{ (Euler's constant)} \quad (37)$$

$$K_n(w) \cong (1/2)(n-1)!(2/w)^n \qquad n \geq 1. \quad (38)$$

For large w it approaches the expression

$$K_n(w) \cong (\pi/zw)^{1/2} \exp\{-w\}. \quad (39)$$

For small values of u the Bessel function can be approximated as

$$J_n(u) \cong (u/2)^n/n! \quad (40)$$

The quantities (u/a) and (w/a) in (26) to (29) are related to the propagation constant h by

$$(u/a)^2 = k_1^2 - h^2 \quad (41)$$

$$(w/a)^2 = h^2 - k_2^2 \quad (42)$$

where k_1 and k_2 are defined by the relation

$$k^2 = \omega^2 \mu\epsilon = \omega^2 \mu_0 \epsilon. \quad (43)$$

Adding (41) and (42) gives

$$(u/a)^2 + (w/a)^2 = k_1^2 - k_2^2 = \omega^2 \mu_0 (\epsilon_1 - \epsilon_2). \quad (44)$$

Define the parameter v by

$$v^2 = u^2 + w^2. \quad (45)$$

Substituting (45) into (44) gives

$$v = \omega a \sqrt{\mu_0(\epsilon_1 - \epsilon_2)} = 2\pi v a \sqrt{\mu_0 \epsilon_0} \sqrt{\epsilon_1' - \epsilon_2'} \quad (46)$$

where v is the frequency in cycles per second and where ϵ' is given by $\epsilon' = \epsilon/\epsilon_0$ and represents the dielectric constant. Since the speed of light c is given by $c = 1/\sqrt{\mu_0 \epsilon_0}$ and the wavelength λ is given by $\lambda = c/v$, (46) can be expressed as

$$v = 2\pi \sqrt{\epsilon_1' - \epsilon_2'}\,(a/c) v = 2\pi \sqrt{\epsilon_1' - \epsilon_2'}\,(a/\lambda). \quad (47)$$

Thus we see that the parameter v is proportional to frequency v and may be considered to be a normalized frequency variable.

The transverse components of the field can be expressed as follows in terms of the longitudinal components [2]:

$$E_r = i[h/(k^2 - h^2)][(\partial E_z/\partial r) + (\mu\omega/h)(1/4)(\partial H_z/\partial \theta)] \quad (48)$$

$$E_\theta = i[h/(k^2 - h^2)][(1/r)(\partial E_z/\partial \theta) - (\mu\omega/h)(\partial H_z/\partial r)] \quad (49)$$

$$H_r = i[h/(k^2 - h^2)][-(k^2/\mu\omega h)(\partial E_z/\partial \theta) + (\partial H_z/\partial r)] \quad (50)$$

$$H_\theta = i[h/(k^2 - h^2)][-(k^2/\mu\omega h)(\partial E_z/\partial r) + (1/r)(\partial H_z/\partial \theta)]. \quad (51)$$

At the boundary $r=a$, the tangential components of E and H must be continuous. Applying this requirement to (26) to (29) and (48) to (51) gives the following transcendental equation that must be satisfied for each mode [2]:

$$(\eta_1+\eta_2)(k_1^2\eta_1+k_2^2\eta_2)=n^2h^2(1/u^2+1/w^2)^2 \quad (52)$$

where

$$\eta_1=[J_n'(u)/uJ_n(u)],\quad \eta_2=[K_n'(w)/wK_n(w)]. \quad (53)$$

By (35), (36), (31), and (32) these quantities can be expressed as

$$\eta_1=J_{n-1}/uJ_n-n/u^2=-J_{n+1}/uJ_n+n/u^2 \quad (54)$$

$$\eta_2=-K_{n-1}/wK_n-K_{n+1}/wK_n+n/w^2. \quad (55)$$

Divide (52) by k_1^2

$$(\eta+\eta_2)[\eta_1+(k_2/k_1)^2\eta_2]=n^2(h/k_1)^2(1/u^2+1/w^2)^2. \quad (56)$$

By (43) the expression $(k_2/k_1)^2$ is equal to ϵ_2'/ϵ_1'. By (41) the expression $(h/k_1)^2$ is equal to

$$(h/k_1)^2=1-(u/ak_1)^2. \quad (57)$$

We also note that by (45) and (44)

$$v^2=a^2(k_1^2-k_2^2)=(ak_1)^2(1-\epsilon_2/\epsilon_1). \quad (58)$$

Combine (57) and (58) and substitute the result into (56). This gives

$$(\eta_1+\eta_2)[\eta_1+(\epsilon_2/\epsilon_1)\eta_2]=n^2[1-(u/v)^2(1-\epsilon_2/\epsilon_1)](1/u^2+1/w^2). \quad (59)$$

Define the parameter δ as follows:

$$\delta=(\epsilon_1-\epsilon_2)/\epsilon_1. \quad (60)$$

Equation (59) then becomes

$$(\eta_1+\eta_2)[\eta_1+(1-\delta)\eta_2]=n^2[1-\delta(u/v)^2](1/u^2+1/w^2)^2. \quad (61)$$

For the case of $n=0$, (61) reduces to the following two simple sets of solutions, which characterize the TE and TM modes:

$$-\eta_1=\eta_2 \qquad \text{TE}_{0m}\text{ modes} \quad (62)$$

$$-\eta_1=(1-\delta)\eta_2 \qquad \text{TM}_{0m}\text{ modes.} \quad (63)$$

By (54) and (55), these are equivalent to

$$-\frac{J_1(u)}{uJ_0(u)}=\frac{K_1(w)}{wK_0(w)} \qquad \text{TE}_{0m}\text{ modes} \quad (64)$$

$$-\frac{J_1(w)}{uJ_0(w)}=\frac{(1-\delta)K_1(w)}{wK_0(w)} \qquad \text{TM}_{0m}\text{ modes.} \quad (65)$$

The TE modes are called transverse electric modes, because the electric E field is completely transverse. In other words, there is no longitudinal component of the E field ($E_z=0$). Similarly, the TM modes are called transverse magnetic modes, because the magnetic H field is completely transverse ($H_z=0$).

The following is a proof that these conditions hold for TE and TM modes. From (26) to (29) and (48) to (51), the continuity of tangential components of E at the boundary $r=a$ requires for $n=0$

$$A_0J_0(u)=C_0K_0(w) \quad (66)$$

$$\frac{B_0J_0'(u)}{u}=\frac{-D_0K_0'(w)}{w}. \quad (67)$$

Continuity of tangential components of H requires that

$$B_0J_0(u)=D_0K_0(w) \quad (68)$$

$$\frac{A_0k_1^2J_0'(u)}{u}=\frac{C_0k_2^2K_0'(w)}{w}. \quad (69)$$

There are two sets of solutions that satisfy these equations, corresponding to the TE modes and TM modes. These solutions are:

TE Modes

$$A_0=C_0=0 \quad (70)$$

$$\frac{J_0'(u)}{uJ_0(u)}=-\frac{K_0'(\omega)}{wK_0(\omega)} \quad (71)$$

TM Modes

$$B_0=D_0=0 \quad (72)$$

$$\frac{J_0'(u)}{uJ_0(u)}=-\frac{K_0'(w)(k_2^2k_1^2)}{wK_0(w)}=-\frac{(1-\delta)K_0'(w)}{wK_0(w)}. \quad (73)$$

By (35) and (36), (71) and (73) can be shown to be equivalent to (64) and (65). The coefficients A_0 and C_0 define the longitudinal E field, and the coefficients B_0 and D_0 define the longitudinal H field. Thus, the TE modes have no longitudinal E field, and the TM modes have no longitudinal H field.

Now let us consider the more complicated case where $n>0$. When there are small differences between the dielectric constants of the core and cladding, we can approximate (61) by setting δ equal to zero. The equation then becomes

$$\eta_1+\eta_2=\pm n(1/u^2+1/w^2) \quad (74)$$

This gives two sets of solutions. We will call the modes corresponding to the plus sign the EH modes and those corresponding to the minus sign the HE modes. A discussion of the basis for this terminology is given by Snitzer [2]. Substituting (54), (55), (31), and (27) into (74) gives for these two sets of solutions

$$-\frac{J_{n+1}(u)}{uJ_n(u)}=\frac{K_{n+1}(w)}{wK_n(w)} \qquad \text{EH modes } (n>0) \quad (75)$$

$$\frac{J_{n-1}(u)}{uJ_n(u)}=\frac{K_{n-1}(w)}{wK_n(w)} \qquad \text{HE modes } (n>0). \quad (76)$$

If we note that $u^2+w^2=v$ we can solve (64), (65), (75), and (76) for u and w as a function of the normalized frequency v for each of the modes.

The right-hand expressions of (64), (65), (75), and (76) are always positive and decay monotonically to zero with increasing w. The left-hand expressions oscillate between $\pm\infty$ as u changes. For each cycle of oscillation the value of u varies over a limited range, but the value of w varies from zero to infinity, and the normalized frequency v varies from cutoff to infinity. Therefore, each cycle defines a different mode and is characterized by a particular value of m.

When w is equal to zero, v is equal to u and we have the lowest frequency v at which the particular mode can exist, for other values of w the frequency v will have a greater value; hence the value of v for which $w=0$ represents the normalized cutoff frequency for that mode. To determine the cutoff frequencies for the modes we can replace the Hankel functions in (64), (65), (75), and (76) by the approximations given in (37) and (38) which hold for small w. From these approximations we find that

$$\frac{K_{n+1}}{wK_n} \to \infty \qquad \text{as } w \to 0 \tag{77}$$

$$\frac{K_{n-1}}{wK_n} \to \infty \qquad \text{as } w \to 0, \quad \text{for } n = 0, 1 \tag{78}$$

$$\frac{K_{n-1}}{wK_n} \to \frac{1}{2(n-1)} \qquad \text{as } w \to 0, \quad \text{for } n \geq 2. \tag{79}$$

Hence from (64), (65), (75), and (76) we have as $w \to 0$

$$\frac{-J_1}{uJ_0} \to \infty \qquad \text{TE, TM modes} \tag{80}$$

$$\frac{-J_{n+1}}{uJ_n} \to \infty \qquad \text{EH modes} \tag{81}$$

$$\frac{J_0}{uJ_1} \to \infty \qquad \text{HE modes } n = 1 \tag{82}$$

$$\frac{J_{n-1}}{uJ_n} \to \frac{1}{2(n-1)} \qquad \text{HE modes, } n \geq 2. \tag{83}$$

If we replace n by $(n-1)$ in (31) we have

$$J_n + J_{n-2} = \frac{2(n-1)J_{n-1}}{u} \tag{84}$$

Substituting this into (83) gives

$$\frac{J_{n-1}}{uJ_n} = \frac{J_{n-2}}{2(n-1)J_n} + \frac{1}{2(n-1)} - \frac{1}{2(n-1)} \tag{85}$$

which is equivalent to

$$\frac{J_{n-2}}{J_n} \to 0. \tag{86}$$

As w approaches zero, v approaches u, and u approaches the normalized cutoff frequency. Hence by (80), (81), (82), and (86), the cutoff frequencies v are given by

$$J_0(v) = 0 \qquad \text{TE, TM modes} \tag{87}$$

$$J_n(v) = 0, \quad v > 0 \qquad \text{EH modes} \tag{88}$$

$$J_1(v) = 0 \qquad \text{HE modes, } n = 1 \tag{89}$$

$$J_{n-2}(v) = 0, \quad v > 0 \qquad \text{HE modes, } n \geq 2. \tag{90}$$

If we substitute into (80), (81), (82), and (86) the Bessel-function approximation for small u of (40), we find that there is only one mode that has a cutoff at $u=v=0$, which is an HE mode for $n=1$, as indicated by (89). This is designated the HE_{11} mode and is the mode that is above cutoff for all frequencies.

These expressions for the cutoff frequencies of the modes hold for $\delta=0$. If the value of δ is greater than zero, the expressions for the cutoff frequencies for the HE modes for $n \geq 2$ change, but the others do not. It can be shown that the cutoff frequency for this case is given by

HE modes, $n \geq 2$

$$J_{n-2}(v) = -[\delta/(2+\delta)]J_n(v), \qquad v > 0 \tag{91}$$

which is the same as (90) for $\delta=0$. Snitzer [2] gives an approximation in this value, which is slightly different. Equation (91) is exact. Table I lists, in the second column, the expressions for the cutoff frequencies for the various modes.

For a given mode, the argument u has its minimum value at cutoff (where it is equal to the normalized cutoff frequency v), and it has its maximum value at infinite frequency. To determine this maximum value of u, let w approach infinity. Equation (39) shows that

$$\frac{K_{n+1}}{wK_n} \to 0, \qquad \frac{K_{n-1}}{wK_n} \to 0 \quad \text{as } w \to \infty. \tag{92}$$

Substituting these into (64), (65), (75), and (76) gives as $w \to \infty$,

$$\frac{J_1}{uJ_n} \to 0 \qquad \text{TE, TM modes} \tag{93}$$

$$-\frac{J_{n+1}}{uJ_n} \to 0 \qquad \text{EH modes} \tag{94}$$

$$\frac{J_{n-1}}{uJ_n} \to 0 \qquad \text{HE modes.} \tag{95}$$

Therefore the values of u at infinite frequency are given by

$$J_1(u) = 0 \qquad \text{TE, TM modes} \tag{96}$$

$$J_{n+1}(u) = 0 \qquad \text{EH modes} \tag{97}$$

$$J_{n-1}(u) = 0 \qquad \text{HE modes.} \tag{98}$$

Snitzer shows that these same expressions hold for all values of δ. This result is summarized in the third column of Table I.

Snitzer [2] shows that for small values of δ the energy flow per unit area in the z direction is circularly sym-

TABLE I
RELATIONS DEFINING CHARACTERISTICS OF VARIOUS DIELECTRIC WAVEGUIDE MODES

Mode		Cutoff Frequency v (Minimum u)	Argument u at Infinite Frequency (Maximum u)	Energy Density (Approximation for Small δ)	
				Inside Core ($r < a$)	Inside Cladding ($r > a$)
TE_{0m}, TM_{0m}		$J_0(v) = 0$	$J_1(u) = 0$	$\left[\frac{J_1(ur/a)}{J_1(u)}\right]^2$	$\left[\frac{K_1(wr/a)}{K_1(w)}\right]^2$
EH_{nm}, $n \geq 1$		$J_n(v) = 0$, $v > 0$	$J_{n+1}(u) = 0$	$\left[\frac{J_{n+1}(ur/a)}{J_{n+1}(u)}\right]^2$	$\left[\frac{K_{n+1}(wr/a)}{K_{n+1}(w)}\right]^2$
HE_{nm}	$n = 1$	$J_n(v) = 0$	$J_{n-1}(u) = 0$	$\left[\frac{J_{n-1}(ur/a)}{J_{n-1}(u)}\right]^2$	$\left[\frac{K_{n-1}(wr/a)}{K_{n-1}(w)}\right]^2$
	$n \geq 2$	$J_{n-2}(v) = \delta J_n(v)/(2 + \delta)$, $v > 0$			

metric with a radial dependence proportional to $J_{n\pm1}^2(ur/a)$, where the plus sign holds for the E modes and the minus sign for the H modes. This expression also holds for the TE and TM modes. Either sign can be considered to apply because the result is the same for $n=0$. Let us assume that for a particular mode the input energy is adjusted such that the energy density S is unity at the boundary. The energy density then can be expressed as

$$S^{(i)}(r) = \left[\frac{J_{n+1}(ur/a)}{J_{n+1}(u)}\right]^2 \quad \text{EH modes} \tag{99}$$

$$S^{(i)}(r) = \left[\frac{J_{n-1}(ur/a)}{J_{n-1}(u)}\right]^2 \quad \text{HE modes} \tag{100}$$

where the superscript (i) on S denotes the energy density inside the core. It also can be shown that for small values of δ the energy flow in the z direction per unit area outside the core is also approximately circularly symmetric with a radial dependence proportional to $K_{n+1}^2(ur/a)$, where the plus sign holds for EH modes and the minus sign holds for HE modes. For small values of δ it can be shown that there is not much change of energy density across the boundary between the core and cladding. Thus for small δ,

$$S^{(i)}(a) \cong S^{(o)}(a) \tag{101}$$

where the superscript (o) applies to the energy density outside the core. By applying this relation it is seen that the energy density expressions in the cladding corresponding to the modes shown in (99) and (100) are

$$S^{(o)}(r) = \left[\frac{K_{n+1}(wr/a)}{K_{n+1}(w)}\right]^2 \quad \text{EH modes} \tag{102}$$

$$S^{(o)}(r) = \left[\frac{K_{n-1}(wr/a)}{K_{n-1}(w)}\right]^2 \quad \text{HE modes.} \tag{103}$$

It is convenient to define the efficiency η of a mode as the per unit amount of energy propagating within the core. By (99) to (103) the efficiency is given by

$$\eta = \frac{\int_0^1 [J_{n\pm1}(ux)J_{n\pm1}(u)]^2 x\,dx}{\int_0^1 [J_{n\pm1}(ux)/J_{n\pm1}(u)]x\,dx + \int_1^\infty [K_{n\pm1}(wx)/K_{n+1}(w)]x\,dx} \tag{104}$$

where the plus sign holds for EH modes, and the minus sign holds for HE modes. The last two columns of Table I list the expressions for the energy densities for the modes inside and outside the core. Equations (99) to (104) apply to the TE and TM modes. The sign makes no difference for $n=0$.

An examination of Table I shows that for $\delta=0$ the following groups of modes have the same values of cutoff frequency v, argument u at infinite frequency, and energy density relations:

$$TE_{0m} \sim TM_{0m} \sim HE_{2m} \tag{105}$$

$$HE_{nm} \sim EH_{(n-2)m} \quad \text{for } n \geq 2. \tag{106}$$

It can be shown that for these modes at $\delta=0$ the plots of u vs. v for each group of modes are the same. Hence, at any given frequency one mode of a group will give exactly the same energy density distribution as the other modes. However, the modes are not exactly the same because they have different E and H field patterns. For $\delta>0$ the mode patterns are different.

Equations have been presented for calculating the values of u and w as functions of the normalized frequency v for the condition of $\delta=0$. Now let us extend this approach to obtain the values for other values of δ. Solve (61) for δ, which gives

$$\delta = \frac{[\eta_1+\eta_2+n(1/u^2+1/w^2)][\eta_1+\eta_2-n(1/u^2+1/w^2)]}{\eta_2(\eta+\eta_2)-(n/w)^2(1/u^2+1/w^2)}. \tag{107}$$

This can be expressed in the following form, which shows that $\delta=0$ for the conditions of (75) or (76) hold:

$$\delta = \frac{\left(\frac{J_{n+1}}{uJ_n}+\frac{K_{n+1}}{wK_n}\right)\left(\frac{J_{n-1}}{uJ_n}-\frac{K_{n-1}}{wK_n}\right)}{\frac{n}{w^2}\left(\frac{J_{n-1}}{uJ_n}\right)+\frac{n}{u^2}\left(\frac{K_{n-1}}{wK_n}\right)-\frac{K_{n-1}}{wK_n}\left(\frac{J_{n+1}}{uJ_n}+\frac{K_{n+1}}{wK_n}\right)} \tag{108}$$

where J and η_1 are functions of u and where K and η_2 are functions of w. Solve (75) and (76) along with $v^2=u^2+w^2$ to get values of u and w at $\delta=0$ for specific values of normalized frequency v for each mode. Then decrease w slightly while keeping u fixed, and calculate the value of δ given in (108). (The value of w should be decreased because this results in positive values of δ.) This procedure gives values of δ vs. w for the particular value of u. Interpolating between these values gives the values of w for specific values of δ at the particular value of u. Since $v^2=u^2+w^2$, we can obtain from this data the values of v vs. u for specific values of δ, which provides the generalized curves of u vs. v for the mode.

Appendix B

Method of Calculation

The curves were calculated on a digital computer by a simple and efficient approximation procedure. This appendix outlines that procedure.

The first step was to calculate u vs. v for $\delta=0$ for the EH and HE modes and for all δ for the TE and TM modes. By (64), (65), (75), (76), and (45), the equations to solve are

$$-\frac{J_1(u)}{uJ_0(u)}=\frac{K_1(w)}{wK_0(w)} \quad \text{TE}_{0m} \text{ modes (all } \delta) \tag{109}$$

$$-\frac{J_1(u)}{(1-\delta)uJ_0(u)}=\frac{K_1(w)}{wK_0(w)} \quad \text{TM}_{0m} \text{ modes (all } \delta) \tag{110}$$

$$-\frac{J_{n+1}(u)}{uJ_n(u)}=\frac{K_{n+1}(w)}{wK_n(w)} \quad \text{EH}_{nm} \text{ modes } (\delta=0) \tag{111}$$

$$\frac{J_{n-1}(u)}{uJ_n(u)}=\frac{K_{n-1}(w)}{wK_n(w)} \quad \text{HE}_{nm} \text{ modes } (\delta=0) \tag{112}$$

$$v^2=u^2+w^2. \tag{113}$$

The procedure was to pick a value of u and solve the left-hand side of (109) to (112). The corresponding value for w was calculated. The values of u and w were then applied to (113) to calculate the normalized frequency v.

To simplify the calculations, tables of $J_n(u)$ and $K_n(w)$ were read into the computer for small equal increments of u and w in the region of interest. From the values of K_n, corresponding tables were formed of $(K_{n\pm1}/wK_n)$. To solve (109) to (112), a table look-up procedure was used. From the value of u, the value of the function $(J_{n\pm1}/uJ_n)$ was found in accordance with (109) to (112). This was related to the table of values of $(K_{n\pm1}/wK_n)$, and the corresponding value for w was found. Linear interpolation was used to find intermediate values of w between those used in the table.

Equation (107) gives the parameter δ as a function of u and w. This equation was used to calculate u vs. v for various values of δ as follows.

First, a particular value of u was chosen. The previous calculations provided the corresponding value for w at which δ is zero. When w is made less than this value, with u held constant, the value of δ becomes greater than zero. The value for δ was calculated repeatedly as w was decreased by equal increments below its original value, with u held constant. By interpolation, the plot of δ vs. w, for constant u, was converted to a plot of w vs. δ, for equal increments of δ, at constant u. By means of (30), these data were then converted to plots of u vs. v for specific values of δ.

Thus, by means of interpolation and table look-up procedures, the computer program was very simple and fast and provided accuracy that was more than adequate for the application.

References

[1] Stratton, J. A., *Electromagnetic Theory*. New York: McGraw-Hill, 1941.
[2] Snitzer, E., *J. Opt. Soc. Amer.*, vol 51, May 1961, p 491–498.
[3] Enoch, J. M., *J. Opt. Soc. Amer.*, vol 51, Oct 1961, p 1122–1126.
[4] Enoch, J. M., *J. Opt. Soc. Amer.*, vol 53, Jan 1963, p 71–85.
[5] Biernson, G., *Proc. San Diego Symposium for Biomedical Engineering*, 1964, p 63.
[6] Jahnke, E., and F. Emde, *Tables of Functions*. New York: Dover, 1945, pp 154–163 and pp 236–243.